NANO LETTERS

2004
Vol. 4, No. 7
1241−1246

Transition Metal Oxide Core–Shell Nanowires: Generic Synthesis and Transport Studies

Song Han, Chao Li, Zuqin Liu, Bo Lei, Daihua Zhang, Wu Jin, Xiaolei Liu, Tao Tang, and Chongwu Zhou*

Department of E.E.-Electrophysics, University of Southern California, Los Angeles, California 90089

Received April 9, 2004; Revised Manuscript Received May 5, 2004

ABSTRACT

A generic non-equilibrium synthesis technique has been developed to produce novel transition metal oxide nanowires, including $YBa_2Cu_3O_{6.66}$, $La_{0.67}Ca_{0.33}MnO_3$, $PbZr_{0.58}Ti_{0.42}O_3$, and Fe_3O_4. Key to our success is the growth of vertically aligned single-crystalline MgO nanowires, which worked as excellent templates for epitaxial deposition of the desired transition metal oxides and led to high-quality core–shell nanowires. Transport studies on $La_{0.67}Ca_{0.33}MnO_3$ nanowires have revealed the remarkable persistence of metal–insulator transition and magnetoresistance down to nanometer scale. Our technique will enable various in-depth studies such as phase transition in nanoscale oxides and may pave the way for novel applications of these fascinating materials.

Transition metal oxides exhibit a rich collection of interesting and intriguing properties ranging from high T_c superconductivity,[1] colossal magnetoresistivity,[2] ferroelectricity,[3] and ferromagnetic properties.[4] These properties can be tailored for a wide variety of applications such as low-loss power delivery,[5] quantum computing using cooper pairs,[6] ultrahigh-density magnetic data storage,[7] and more recently spintronic applications.[8] Many transition metal oxides have been prepared in bulk form or as thin films,[9−13] which paved the way for intensive research studies in the past several decades. Inspired by the above-mentioned success, we expect that nanostructures, in particular, nanowires made of transition metal oxides may offer enormous opportunities to explore intriguing physics and also practical applications. The past decade has witnessed tremendous progress toward synthesis of nanowires[14] using techniques including the vapor−liquid−solid (VLS) approach,[15] chemical synthesis,[16] the solvothermal method, and template directed synthesis.[17] These techniques have produced mostly semiconductive nanowires for applications such as nanocircuits[18] and nanolasers.[19] In contrast, the synthesis of transition metal oxide nanowires has seen success with only a few material systems such as $BaTiO_3/SrTiO_3$ nanorods,[20] $Co_{0.05}Ti_{0.95}O_2$ nanotapes,[21] and more recently $(La,Sr)MnO_3$ nanorods.[22] Such limited effort is largely related to the complex composition of transition metal oxides, and most techniques (e.g., the VLS approach) developed in the past for semiconductive nanowires cannot be applied due to issues such as phase separation and the lack of suitable catalysts.[23] In contrast, non-equilibrium deposition techniques may serve to preserve the material composition and have been employed to produce core−shell nanowires based on Si/Ge systems[24] and also $Co_{0.05}Ti_{0.95}O_2@SnO_2$ nanotapes.[21]

We have developed a generic non-equilibrium synthesis technique to produce a wide variety of core−shell transition metal oxide nanowires, including $YBa_2Cu_3O_{6.66}$ (YBCO), $La_{0.67}Ca_{0.33}MnO_3$ (LCMO), $PbZr_{0.58}Ti_{0.42}O_3$ (PZT), and Fe_3O_4. These four material systems represent a broad collection of physical properties: YBCO is a well-known high T_c superconductor,[9] LCMO exhibits intriguing colossal magnetoresistance,[10] PZT is an important ferroelectric material,[12] and Fe_3O_4 is a spin half-metal which is under intensive studies.[13] Key to our success is the preparation of vertically aligned MgO nanowires to work as the core material. These vertical nanowires were then used as templates for pulsed laser deposition (PLD) of the desired transition metal oxides by building upon the knowledge accumulated in the past decades on metal oxide film studies.[25] This technique yielded single crystalline core−shell MgO/transition metal oxide nanowires with precisely controlled layer thickness. Transport studies on a 10 nm thick LCMO nanowire have revealed pronounced magnetoresistance with a transition temperature ∼170 K and magnetoresistance ratio approaching 70%. Our technique will enable phase transition studies in nanoscale transition metal oxide nanowires and may pave the way for various novel applications.

We first developed a novel method to produce vertical arrays of single crystalline MgO nanowires following the vapor−liquid−solid mechanism.[23] Our system consists of a

* Corresponding author. E-mail: chongwuz@usc.edu.

10.1021/nl049467o CCC: $27.50
Published on Web 06/03/2004

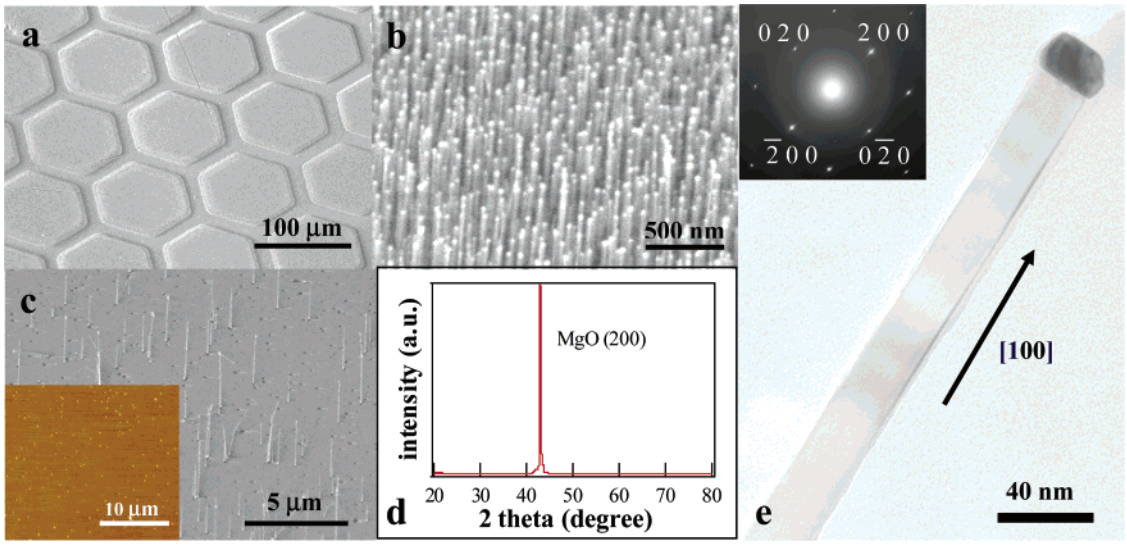

Figure 1. Synthesis of MgO nanowires by chemical vapor deposition. (a) Low-magnification SEM image of MgO nanowires grown on MgO (100) substrate. 1 nm gold film was evaporated through a TEM grid and used as the catalyst. (b) Higher magnification SEM image of the sample showing nanowires standing normal to the substrate. (c) SEM image of MgO nanowires grown with 30 nm gold clusters as catalyst. Inset: AFM image of gold clusters before the growth. (d) XRD data of MgO nanowires grown on a MgO (100) substrate. (e) TEM image of an individual MgO nanowire. Inset: Nanowire diffraction pattern. The nanowire was identified to grow along [100] direction.

horizontal quartz tube furnace, which hosts a ceramic boat filled with Mg_3N_2 powder working as the feedstock. Single crystalline (100) MgO substrates coated with Au nanoclusters were put downstream of the Mg_3N_2 powder. The furnace was then heated to 900 °C with Ar mixed with a trace amount of oxygen flowing at 100 sccm all the time. After cooling, the MgO substrates appeared rough compared to the smooth surface before the growth. The as-grown product was then characterized by scanning electron microscopy (SEM), energy-dispersive X-ray spectroscopy (EDS), X-ray diffraction (XRD), transmission electron microscopy (TEM), and high-resolution TEM (HRTEM).

We have prepared the gold nanoclusters using two methods. First, e-beam evaporation was used to coat the MgO substrates with 1 nm gold film, and a TEM grid was used as a shadow mask. Figure 1a depicts a low-magnification SEM image of the nanowires grown with the patterned Au film. MgO nanowires grew only within the hexagonal regions where Au films were deposited, indicating that gold worked as the catalyst. Figure 1b shows a high-magnification image of the same sample, and all the nanowires were observed to stand normal to the substrate with the gold catalytic particles showing at the tips as bright spots. These nanowires are typically several microns long and 30−100 nm in diameter. To gain further control over the nanowire diameter and also the array density, we also prepared MgO (100) substrates coated with monodispersed gold clusters of 30 nm in diameter (Figure 1c inset), and an SEM image of the substrate after the MgO nanowire growth is presented in Figure 1c. It clearly shows that these nanowires have uniform diameters and essentially all stand normal to the substrate. The density of nanowires is in good agreement with the density of catalysts. The length of the nanowires can be controlled by tuning the reaction time, and a typical growth rate of 0.3−0.5 μm/min was found for our synthesis. X-ray diffraction was carried out over such samples, and only one diffraction peak corresponding to the MgO (200) plane was detected (Figure 1d). This is a direct result of the epitaxial nature of the interface between our nanowires and the MgO substrates, and thus confirmed that we obtained single-crystalline nanowires with [100] as the growth direction. This is further confirmed by a detailed TEM analysis shown in Figure 1e, and the nanowires are always found to be smooth, uniform, and defect-free. Moreover, the nanowire terminates in a cluster similar in size to the nanowire diameter, indicating the MgO nanowire growth follows the catalyst-guided vapor−liquid−solid growth mechanism.[23] The select area electron diffraction (SAED) pattern of the MgO nanowire (Figure 1e, inset) reveals that the nearest diffraction spot to the center corresponds to the (200) plane, which is the case for face-center-cubic crystal structures.[26]

Similar to the conventional epitaxial film growth, these MgO nanowires provide a great opportunity to work as templates for other materials. Several advantages are worth mentioning for our MgO vertical nanowire arrays. The first is that these nanowires can be used to grow core−shell nanowires instead of nanotapes.[21,27] These core−shell structures may exhibit intriguing physics, such as destruction of the global phase coherence in ultrathin superconducting cylinders,[28] and may also work as building blocks for more sophisticated core−multishell structures. Second, MgO can work as the substrate for epitaxial growth of a wide variety of interesting materials, including YBCO, PZT, LCMO, and Fe_3O_4, and thus a truly generic approach can be developed. These nanowires are very hard to grow using conventional chemical vapor deposition techniques due to their complex compositions and keen dependence on the temperature and pressure.[29]

Schematic illustrations of MgO nanowires before and after the PLD process are shown in Figure 2a. The laser beam from a pulse mode Nd:YAG laser ($\lambda = 532$ nm) was focused onto a target and the generated plume was then deposited

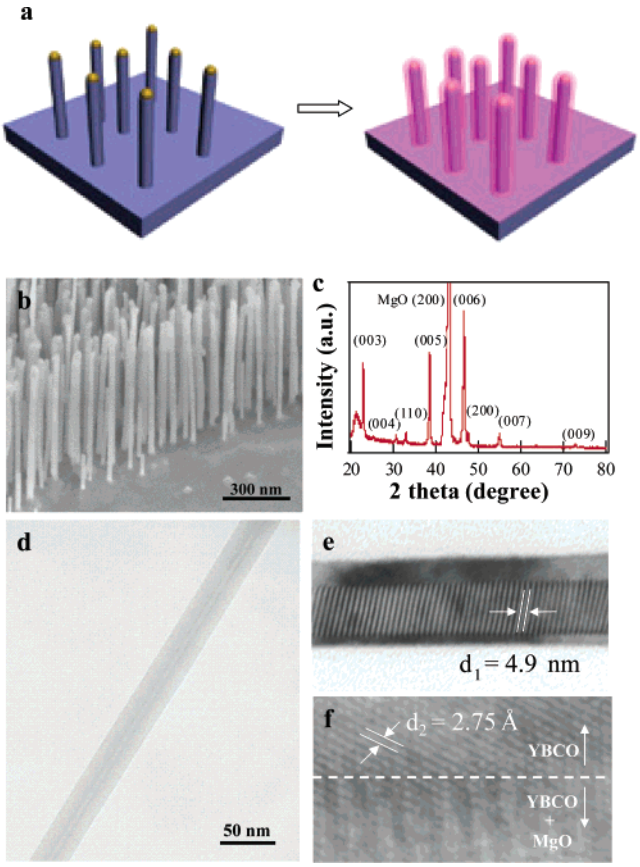

Figure 2. PLD process was applied to synthesize transition metal oxide core−shell nanowires after MgO nanowire growth. (a) Schematic illustration of vertically aligned MgO nanowires before the PLD process and core−shell nanowires consisting of MgO nanowires coated with the desired material after the PLD process. (b) SEM image of YBCO nanowires after the PLD process. (c) XRD data of as-grown YBCO nanowires on a MgO (100) substrate. (d) Low magnification TEM image showing the MgO/YBCO core−shell structure. (e) TEM image of MgO/YBCO nanowire showing parallel Moiré patterns. (f) HRTEM image of the MgO/YBCO nanowire.

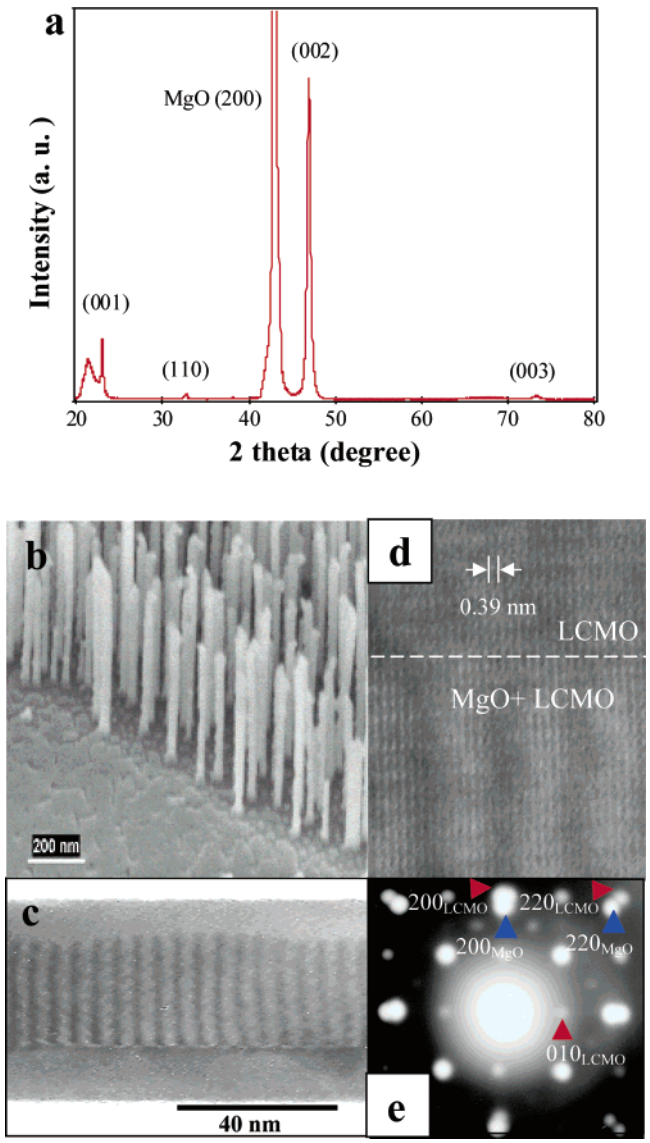

Figure 3. MgO/LCMO core−shell nanowire synthesis. (a) XRD data of the MgO/LCMO core−shell nanowires grown on a MgO substrate. (b) SEM image of LCMO nanowires after the PLD process. (c) TEM image showing the MgO/LCMO core−shell structure and parallel Moiré patterns. (d) HRTEM image of a MgO/LCMO nanowire. (e) SAED pattern of a MgO/LCMO nanowire.

onto a vertical MgO nanowire array sample. The sample temperature, ambient gas, and pressure were carefully tuned to optimize the epitaxial growth of the desired material on the MgO nanowires. One significant advantage of using vertically aligned MgO nanowires as templates is that these nanowires are well separated and do not shadow each other, and hence high-quality conformal coating can be readily achieved to yield core−shell nanowires. Figure 2b shows a SEM image of MgO/YBCO core−shell nanowires grown on a MgO (100) substrate using the PLD approach. Most of the nanowires are still normal to the substrate after the PLD process. Figure 2c shows the XRD pattern of a typical MgO/YBCO sample. In addition to the strong MgO (200) peak, several other peaks were observed and can be indexed to the orthorhombic structure of YBCO. Most of the YBCO peaks correspond to the (00*n*) planes, with *n* being an integer, indicating that the YBCO coating is single-crystal and well-aligned. Weak peaks corresponding to (110) and (200) were also observed and are likely due to the nanowire bending shown in Figure 2b. EDS was performed to determine the ratio between the heavy elements, and a result of 1:2:3 for Y/Ba/Cu was obtained. The oxygen ratio was determined by comparing the lattice constants derived from the aforementioned XRD pattern with the database.[30] These two techniques combined identified the coating layer as $YBa_2Cu_3O_{6.66}$. Furthermore, the core−shell nanowire structure was directly confirmed using low magnification transmission electron microscopy, as shown in Figure 2d. The MgO core can be seen to be 9 nm in diameter and coated with 15 nm thick YBCO conformally. Due to the difference in lattice spacing (MgO: $a_1 = 0.421$ nm and YBCO: $a_2 = 0.382$ nm, $b = 0.388$ nm and $c = 1.169$ nm),[30] overlapping of MgO crystals and YBCO crystals may form periodic beat-like structures and lead to the well-known Moiré pattern in electron microscopy.[31] Moiré patterns (Figure 2e) are observed in the inner region of core−shell nanowires, where overlapping MgO and YBCO lattices exist. In contrast, no

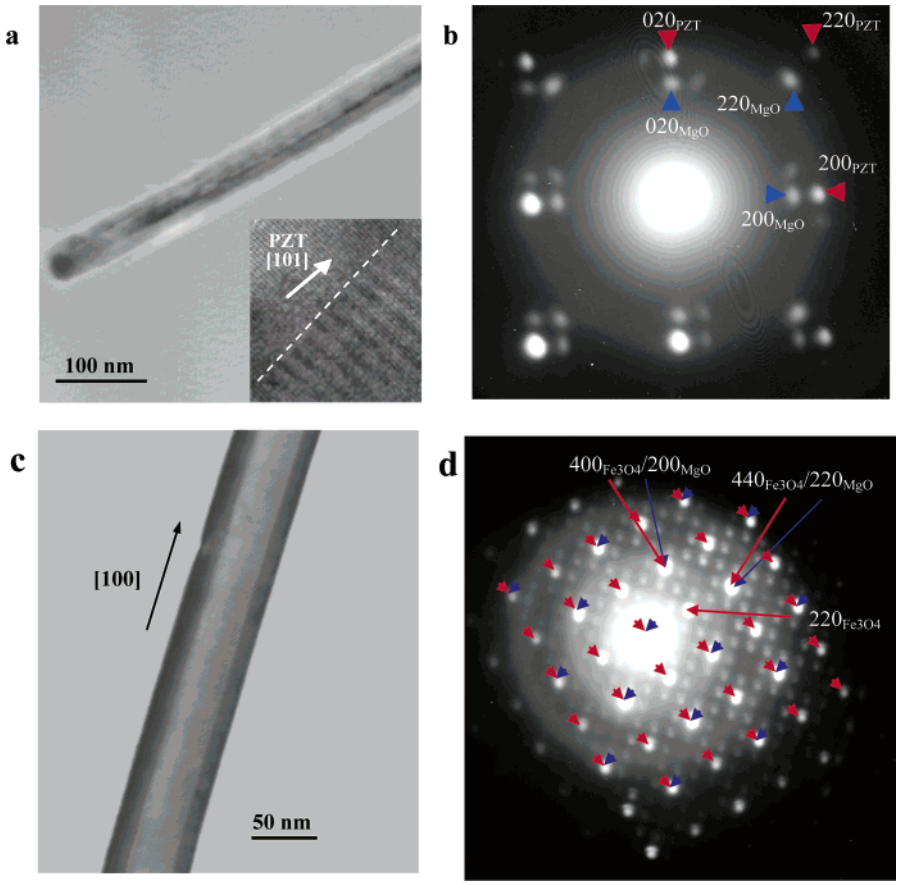

Figure 4. MgO nanowire templates were also used for PZT and Fe_3O_4 core−shell nanowire synthesis. (a) TEM image of a PZT nanowire. The catalyst can be seen at the end of the nanowire. Inset: HRTEM image of the MgO/PZT core−shell nanowire at the sample tilt angle of 45 degrees. (b) SAED pattern of a MgO/PZT nanowire. Red arrows inside are PZT diffraction dots and blue arrows outside are MgO diffraction dots. (c) TEM image of an Fe_3O_4 nanowire. (d) SAED pattern of a MgO/Fe_3O_4 core−shell nanowire. Red and blue arrows indicate Fe_3O_4 and MgO diffraction patterns, respectively. The weak and unmarked spots come from Fe_3O_4.

such beating pattern was observed in the outer region (YBCO only) of the nanowire. The period of the Moiré pattern is determined to be $d_1 = 4.9$ nm, consistent with the value derived from the equation $d_1 = (a_1 \times b)\cos\omega/(a_1 - b)$, where a_1 is the (100) MgO spacing of 0.421 nm, b is (010) YBCO spacing of 0.388 nm, and $\omega = 11.1°$ is the tilt angle of Moiré fringe. From the angle ω, the tilt of (010) YBCO relative to (100) MgO is calculated as 0.9 degree.[31] This indicates that the YBCO nanowire is single crystalline with ⟨010⟩ being the axial direction. The epitaxial nature of the growth was further revealed by the high-resolution TEM image shown in Figure 2f, where the lattice spacing of 2.75 Å between the (110) planes can be clearly resolved for the YBCO shell layer.

A similar synthesis approach can also be applied to MgO/LCMO core−shell nanowires. LCMO is an important material exhibiting colossal magnetoresistance and a metal insulator transition near the critical temperature.[2,10] The synthesis was carried out via PLD to form MgO/LCMO core−shell nanowires with the substrate temperature kept at 800 °C in an ambient of 200 mTorr O_2. The XRD pattern of MgO/LCMO core−shell nanowires is shown in Figure 3a. Several peaks can be identified to correspond to LCMO (001), (110), (002), and (003), in addition to MgO (200) from MgO substrate and MgO nanowires. Figure 3b shows an SEM image of the as-synthesized core−shell nanowires. The core−shell nanowires remain normal to the substrate even after the LCMO deposition. A clear Moiré pattern was also observed for these core−shell nanowires (Figure 3c), with the inner MgO core about 20 nm in diameter and the LCMO shell layer around 10 nm in thickness. Figure 3d shows an HRTEM image taken at the interface between the core and the shell layers. The lattice spacing of 0.39 nm corresponds to LCMO (100) plane, indicating [100] as the axial direction for LCMO TEM image. The electron diffraction pattern shown in Figure 3e also confirms the epitaxial growth, as two sets of diffraction patterns were observed, corresponding to the MgO cubic lattice and the LCMO cubic perovskite lattice. One can further derive [100] as the MgO axial direction and [100] as the LCMO axial direction, consistent with our analysis from the Moiré pattern and the HRTEM image.

Our synthetic technique readily lends itself to other material systems, including PZT, a ferroelectric dielectric,[12] and Fe_3O_4, a spin half-metal.[13] MgO nanowire templates were used for both materials, and the technique details can be found in the Supporting Information. The MgO/PZT core−shell structure can be clearly seen in the TEM image in Figure 4a. Figure 4b reveals two sets of diffraction patterns for MgO and PZT and thus confirms the single-crystal nature

of our core−shell nanowires. TEM analysis also reveals [100] as the axial direction for the PZT shell layer. TEM analysis of the MgO/Fe_3O_4 core−shell nanowires is shown in Figure 4c and 4d. An epitaxial layer of Fe_3O_4 (dark) can be seen uniformly coated around the MgO interior core (light) (Figure 4c). By indexing the corresponding SAED pattern (Figure 4d), the axial direction was identified to be [100] for both MgO and Fe_3O_4. In the figure, the diffraction spots coming from the Fe_3O_4 shell and MgO core were marked with red and blue arrows, respectively (the weak and unmarked spots also come from Fe_3O_4). The ovelapping of the two sets of patterns is attributed to the perfect lattice match between the two materials (mismatch $\sim$ 0.3%).[13] However, because of their difference in the lattice constants (0.839 nm for Fe_3O_4),[13] the patterns showed two spacial periods, with the dense and sparse pattern for Fe_3O_4 and MgO, respectively.

Our synthesis capability renders unique opportunities to study a number of issues of fundamental importance, such as phase transition at nanoscale dimensions. Below we use our study on LCMO nanowires as our example. The as-grown MgO/LCMO core−shell nanowires were first sonicated off the MgO substrate into 2-propanol, and then dispersed onto a Si/SiO_2 substrate by spin coating. E-beam lithography was used to pattern four electrodes, followed by Ag/Au deposition to contact the nanowires. Figure 5a inset shows the SEM image of a typical device with the nanowire around 5 μm in length and contacted by four electrodes. TEM studies performed with nanowires sonicated off the same sample revealed the MgO core and the LCMO shell thickness both being 10 nm. The LCMO resistivity is estimated to be 4.4×10^{-4} Ω-m at room temperature based on four-point probe measurements, consistent with the value obtained from single-crystal film samples.[11] The resistance as a function of temperature was measured both with and without a 1 T magnetic field applied perpendicular to the nanowire long axis. As shown in Figure 5a, the sample underwent a transition from an insulating state ($dR/dT < 0$) to a metallic state ($dR/dT > 0$). There appears a resistance peak around 170 K without the magnetic field. Interestingly, with a 1 T magnetic field, the resistance peak shifted to 180 K. This is understandable as a magnetic field will enhance the spin ordering in the CMR material, and hence the metal insulator transition can be observed at higher temperature.[11] Figure 5b shows the magnetoresistance (MR) measured at 170 K with a magnetic field up to 2 T. The resistance has its maximum value at zero field and was monotonically reduced by higher magnetic field. By defining the MR ratio as $[R(H) - R(2T)]/R(2T) \times 100\%$, a value of 70% was determined, indicating the high quality of the nanowire device. The observed metal−insulator transition and the magnetoresistance unambiguously establish the existence of colossal magnetoresistance in our MgO−LCMO nanowire system. Hole-doped manganites such LCMO are well known to display a remarkable sensitivity to various perturbations such as stress and film thickness. For instance, an absence of metal−insulator transition has been observed for 15 nm LCMO films deposited on (001) $LaAlO_3$ substrates with a lattice mismatch ~2%,[32] while the existence of a dead layer

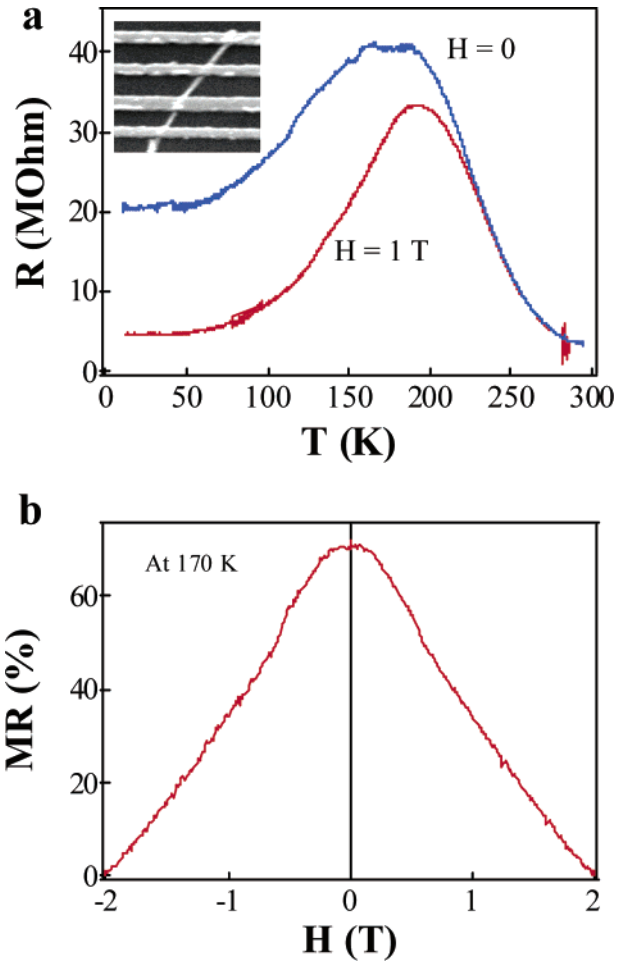

Figure 5. Transport studies on a MgO/LCMO core−shell nanowire. (a) Resistance versus temperature data of a LCMO nanowire measured at $H = 0$ T (red curve) and $H = 1$ T (blue curve). The peak of resistance was measure at 170 K for $H = 0$ T and 180 K for $H = 1$ T. Inset is an SEM image of the device. (b) Magnetoresistance measured at 170 K with a magnetic field swept from −2 T to 2 T.

~20 nm has been reported for epitaxial LCMO films at the interface.[11] The persistence of the metal−insulator transition in our MgO/LCMO core−shell nanowires is therefore truly remarkable, as our LCMO layer is only 10 nm in thickness and the lattice mismatch between bulk MgO and LCMO approaches 9.0%. The origin of our observation awaits further investigation and is likely related to the relaxation of the stress in the radial direction unique to core−shell nanowires. Our observation thus has important implications for functioning transition metal oxide nanowires with desired properties.

In summary, we have presented a versatile synthetic approach to produce various high-quality, single crystalline transition metal oxide nanowires. The spirit of our approach is to use suitable nanowire templates plus pulsed laser deposition of desired materials. Along this direction many other nanowire systems can be developed, for example, by using a wide choice of template materials (for example, ZnO, Al_2O_3, $LiAl_2O_3$, $SrTiO_3$, and $LaAlO_3$) and shell materials (e.g., LSMO, LBMO, $TlBaO_3$, and $LiNbO_3$). These materials carry a wide spectrum of physical, chemical and electronic

properties ranging from superconductivity, ferroelectricity, colossal magnetoresistivity, and nonlinear optical properties, and therefore hold great promise for future applications. Our work also paves the way for core−multishell structures consisting of combinations of the above-mentioned materials. This may lead to novel devices such as ferroelectric gated superconductors[33] and manganites.[34]

Acknowledgment. We thank Prof. Edward Goo for helpful discussions and USC Microscope Center for the use of their facilities. We also thank Dr. Jinping Zhang for the help with the HRTEM. We acknowledge support of this work by a National Science Foundation CAREER Award and Defense Advanced Research Projects Agency.

Supporting Information Available: Detailed experimental information of PLD processes. This material is available free of charge via the Internet at http://pubs.acs.org.

Note Added after ASAP Posting. This article was posted ASAP on 6/3/2004. The equation $[R(0) - R(\mathrm{H})]/R(\mathrm{H}) \times 100\%$, located two paragraphs before the Acknowledgment section, was changed to $[R(\mathrm{H}) - R(2\mathrm{T})]/R(2\mathrm{T}) \times 100\%$. The corrected version was posted on 6/23/2004.

References

(1) Dai, P.; Mook, H. A.; Aeppli, G.; Hayden, S. M.; Doğan, F. *Nature* **2000**, *406*, 965.
(2) Moreo, A.; Yunoki, S.; Dagotto, E. *Science* **1999**, *283*, 2034.
(3) Tybell, T.; Paruch, P.; Giamarchi, T.; Triscone, J.-M. *Phys. Rev. Lett.* **2002**, *89*, 097601.
(4) Prinz, G. A. *Science* **1999**, *282*, 1660.
(5) Lubkin, G. B. *Phys. Today* **1996**, *49*, 48.
(6) Vion, D.; Aassime, A.; Cottet, A.; Joyez, P.; Pothier, H.; Urbina, C.; Esteve, D.; Devoret, M. H. *Science* **2002**, *296*, 886.
(7) Sun, S.; Anders, S.; Thomson, T.; Baglin, J. E. E.; Toney, M. F.; Hamann, H. F.; Murray, C. B.; Terris, B. D. *J. Phys. Chem. B* **2003**, *107*, 5419.
(8) Awschalom, D. D.; Flatté, M. E.; Samarth, N. *Sci. Am.* **2002**, *286*, 66.
(9) Skakle, J. M. S. *Mater. Sci. Eng., R* **1998**, *23*, 1.
(10) Fäth, M.; Freisem, S.; Menovsky, A. A.; Tomioka, Y.; Aarts, J.; Mydosh, J. A. *Science* **1999**, *285*, 1540.
(11) Haghiri-Gosnet, A. M.; Renard, J. P. *J. Phys. D: Appl. Phys.* **2003**, *36*, R127.
(12) Ahn, C. H.; Rabe, K. M.; Triscone, J.-M. *Science*, **2004**, *303*, 488.
(13) Gregg, J. F.; Petej, I.; Jouguelet, E.; Dennis, C. *J. Phys. D: Appl. Phys.* **2002**, *35*, R121.
(14) Xia, Y.; Yang, P. *Adv. Mater*. **2003**, *15*(5), Special Issue: Nanowires.
(15) Wagner, R. S.; Ellis, W. C. *Appl. Phys. Lett.* **1964**, *4*, 889.
(16) Manna, L.; Scher, E. C.; Alivisatos, A. P. *J. Am. Chem. Soc.* **2000**, *122*, 12700.
(17) Xia, Y.; Yang, P.; Sun, Y.; Wu, Y.; Mayers, B.; Gates, B.; Yin, Y.; Kim, F.; Yan, H. *Adv. Mater.* **2003**, *15*, 353.
(18) Zhong, Z.; Wang, D.; Cui, Y.; Bockrath, M. W.; Lieber, C. M. *Science* **2003**, *302*, 1377.
(19) Huang, M. H.; Mao, S.; Feick, H.; Yan, H.; Wu, Y.; Kind, H.; Weber, E.; Russo, R.; Yang, P. *Science* **2001**, *292*, 1897.
(20) Urban, J. J.; Yun, W. S.; Gu, Q.; Park, H. *J. Am. Chem. Soc.* **2002**, *124*, 1186.
(21) He, R.; Law, M.; Fan, R.; Kim, F.; Yang, P. *Nano Lett.* **2002**, *2*, 1109.
(22) Jiang, J.; Henry, L. L.; Gnanasekar, K. I.; Chen, C.; Meletis, E. I. *Nano Lett.* **2004**, *4*, 741−745.
(23) Hu, J.; Odom, T. W.; Lieber, C. M. *Acc. Chem. Res.* **1999**, *32*, 435.
(24) Lauhon, L. J.; Gudiksen, M. S.; Wang, D.; Lieber, C. M. *Nature* **2002**, *420*, 57.
(25) Kwon, C.; Li, Q.; Kim, K. C.; Robson, M. C.; Trajanovic, Z.; Peng, J. L.; Greene, R. L.; Repaci, A. M.; Lobb, C.; Decca, R.; Drew, H. D.; Ramesh, R.; Venkatesan, T.; Ham, K. M.; Sooryakumar, R. *Superlatt. Microstruct.* **1996**, *19*, 169.
(26) Henry, N. F. M.; Lonsdale, K. *International Tables for X-ray Crystallography*, Vol. I.; The Kynoch Press: England, 1952.
(27) Pan, Z. W.; Dai, Z. R.; Wang, Z. L. *Science* **2001**, *291*, 1947.
(28) Liu, Y.; Zadorozhny, Yu.; Rosario, M. M.; Rock, B. Y.; Carrigan, P. T.; Wang, H. *Science* **2001**, *294*, 2332.
(29) Wu, Y.; Yan, H.; Huang, M.; Messer, B.; Song, J.; Yang, P. *Chem. Eur. J.* **2002**, *8*, 1261.
(30) PCPDFWIN. Version 2.02. *International Center for Diffraction Data*; ICDD: Newtown Square, 1999.
(31) Hirsch, P. *Electron microscopy of thin crystals*; Robert E. Krieger Publishing: Malabar, Florida, 1977.
(32) Biswas, A.; Rajeswari, M.; Srivastava, R. C.; Li, Y. H.; Venkatesan, T.; Greene, R. L. *Phys. Rev. B* **2000**, *61*, 9665.
(33) Ahn, C. H.; Gariglio, S.; Paruch, P.; Tybell, T.; Antognazza, L.; Triscone, J. M. *Science* **1999**, *284*, 1152.
(34) Chiba, D.; Yamanouchi, M.; Matsukura, F.; Ohno, H. *Science* **2003**, *301*, 943.

NL049467O